Available online at www.sciencedirect.com
SCIENCE DIRECT®
Journal of Sound and Vibration 264 (2003) 317–342
JOURNAL OF SOUND AND VIBRATION
www.elsevier.com/locate/jsvi

Passive reduction of gear mesh vibration using a periodic drive shaft

D. Richards, D.J. Pines*

Alfred Gessow Rotocraft Center, Department of Aerospace Engineering, University of Maryland, College Park, MD 20742-3015, USA

Received 20 June 2001; accepted 29 June 2002

Abstract

In this paper, a passive approach to reduce transmitted vibration generated by gear mesh contact dynamics is presented. The approach utilizes the property of periodic structural components that creates stop band and pass band regions in the frequency spectra. The stop band regions can be tailored to correspond to regions of the frequency spectra that contain harmonics and sub-harmonics of the gear mesh frequency, attenuating the response in those regions. A periodic structural component is comprised of a repeating array of cells, which are themselves an assembly of elements. The elements may have differing material properties as well as geometric variations. For the purpose of this research, only geometric variations are considered and each cell is assumed to be identical. A periodic shaft is designed and machined in order to reduce transmitted vibration of a pair of spur gears. Analytical and experimental results indicate that transmitted vibrations from gear mesh contact to the bearing supports are reduced at a variety of operational speeds under static torque preload.

1. Introduction

One of the major sources of cabin noise in helicopters can be attributed to gear impact loads that occur during normal operation of a transmission. These loads are caused by a stiffness variation which occurs as gear teeth mesh. Impact load induced vibrations are transferred through the internal components of the gearbox to the housing structure. From there, the vibrations are transferred to the cabin panels through load paths from the gearbox mounting supports. Although there is a high noise level within the gearbox, the air pressure levels inside the gearbox

*Corresponding author. Tel.: +1-301-405-0263; fax: +1-301-314-9001.
E-mail address: djpterp@eng.umd.edu (D.J. Pines).

0022-460X/03/$ - see front matter
doi:10.1016/S0022-460X(02)01213-0

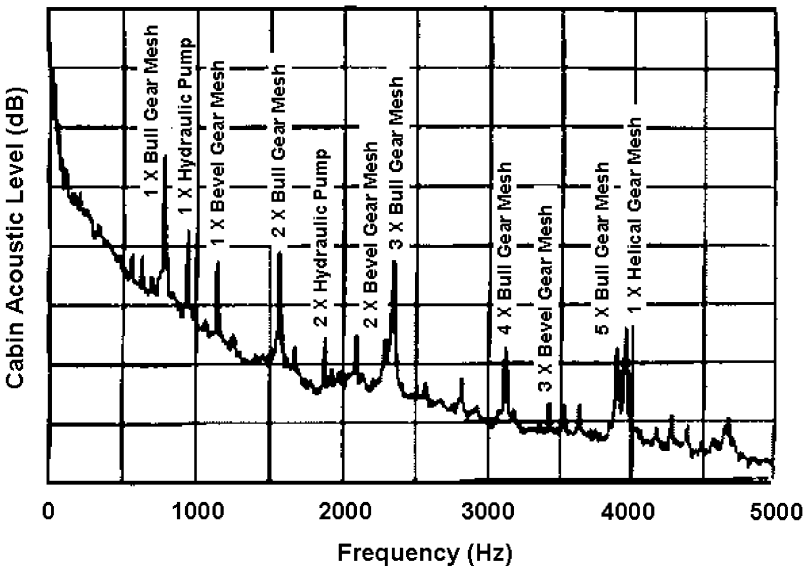

Fig. 1. S-76 gearbox noise spectrum.

are generally not sufficient to excite the housing panels considerably [1]. Thus, the primary source of cabin noise is derived from structure-borne noise generated by gear contact dynamics. Minimizing the effect of these dynamics is complicated by the fact that the vibrations occur at multiple harmonics of the gear mesh frequency. These vibrations generate sound pressure levels inside the cabin that have been measured up to 100 dB in the frequency range of 500–6000 Hz, a frequency range that is important to human speech [2]. Fig. 1 shows the noise spectrum obtained from within the cabin. The acoustic noise level is dominated by peaks which correspond to the mesh frequencies and associated harmonics thereof.

2. Background

There have been a variety of passive methods used to reduce gear noise [5–8]. Much of this work has focused on tooth profile modifications [3,4]. As gear teeth engage, they make contact at the mesh point which travels along the profile of the tooth. Therefore, the torque applied causes a deflection of the teeth which varies as the teeth engage. This translates directly to a mesh stiffness variation. This stiffness change generates a dynamic load which not only reduces the useful torque capacity, but contributes to gear noise. Profile modifications may include tip and/or root relief. In addition, crowning of the tooth profile is possible. All these methods have been shown to reduce dynamic loads on teeth and transmission error, but each has its limitations. For tip/root relief, the dynamic load reduction is torque load specific, implying that there is a certain torque load condition for which the tooth profile is designed. Operating at a torque load which differs from the design load may generate increased transmission error and subsequently higher gear noise [5]. Also, such an approach is sensitive to manufacturing inaccuracies. Crowning is sensitive to inaccuracies as well and can affect torque capacity. Too much crowning may cause the center of

the tooth to be overloaded and produce excessive Hertzian contact stresses. If there is too little crowning, lead error and/or misalignment can cause excessive loads at the end of the tooth, resulting in accelerated fatigue failures [6]. Optimal design of the entire gearbox for low noise was investigated by Inoue et al. [7].

The use of snap rings was investigated by Okamura et al. [8]. This is a simple passive approach in which rings of material are placed within the rim of the gear. The "snap ring" is not a completely enclosed ring. A cut is made in the ring, allowing for the expansion of the ring due to centrifugal forces which generates an increase in contact pressure at the mesh point. This assists in reducing the noise level. They have been shown to work well for helical gears, but the performance for spur gears is minimal.

Active methods have also been used to reduce gearbox vibrations. Researchers have investigated the effectiveness of using piezoelectric actuators integrated to the cabin panels [9,10], the bearing outer race [11], and the gearbox struts [12,13]. The difficulty with these approaches is that they require a large number of actuators and a source of external power. For the gearbox struts, actuators would be needed at each loadpath from the gearbox. Also, the actuators presently available are effective at controlling one harmonic of the gear mesh frequency. Controlling multiple harmonics would require either multiple actuators or a novel control law. The use of magnetic bearings for active control was investigated by Lee and Chen [14–16]. Reduction of torsional waves in a shaft has been investigated passively through profile modification [4] and viscoelastic damping [17], and actively through active constrained layer damping [18].

The passive method investigated in this work attempts to show that the introduction of periodicity into the shaft of a gear system may reduce vibrations transferred along the shaft and therefore prevent gear mesh vibrations from being transmitted into the gearbox bearings and support members. A periodic shaft is comprised of repeating shaft segments with either varying geometry, varying material properties, or some combination thereof. Discontinuities in the shaft scatter the waves as they are encountered and create pass and stop bands in the frequency spectra. This property of the shaft can be used to design stop bands that correspond to particular harmonics of the gear mesh contact dynamics. In this work, the use of a periodic shaft is shown to significantly reduce vibrations associated with spur gear mesh vibrations.

3. A periodic beam model

A periodic structure consists of an assembly of identical elements connected in a repeating array which together form a completed structure. Examples of such structures are found in many engineering applications. These include bulkheads, airplane fuselages, and apartment buildings with identical storeys. Each such structure has a repeating set of stiffeners which are placed at regular intervals. The study of periodic structures has a long history. Wave propagation in periodic systems has been investigated for approximately 300 years [19]. Typically, the studies have been related to crystals, optics, and the like. It is only recently that the wave motion in periodic structures has been studied. The salient feature of such structures is the fact that waves can propagate through the structure in some frequency bands (pass bands) and not in others (stop

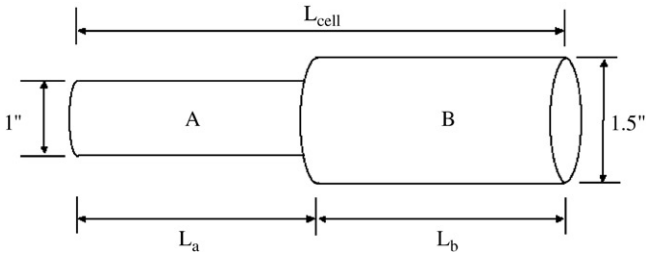

Fig. 2. Shaft geometry.

bands) [20–25]. The present work focuses on the application to a spur gear pair system and the prevention of the propagation of waves transmitted through the shaft into the bearings and supports.

Spectral finite element analysis [26] will be used to analyze the shaft vibrations (both torsional and transverse vibrations) and determine the propagation parameter, μ. This parameter indicates the regions for which there is attenuation of the vibrations transmitted through the structure (stop bands) and where waves are allowed to transmit energy (pass bands) [27,28].

This section will begin with the development of spectral finite element analysis for transverse vibrations of a beam will be developed and the effect of geometrical changes in the cell structure will be presented. Finally, the inclusion of the gear inertia on transverse beam dynamics with a finite length and pinned boundary conditions will be presented.

For a beam (see Fig. 2), the equation of motion may be shown to be (neglecting the rotational inertia term $\rho I\ddot{\phi}$ and considering a beam section with uniform properties)

$$EIv'''' + \rho A\ddot{v} = 0 \tag{1}$$

which has the solution

$$v(x,\omega) = a_1 e^{-ikx} + a_2 e^{ikx} + a_3 e^{-kx} + a_4 e^{kx} \tag{2}$$

with

$$a = \{\, a_1 \quad a_2 \quad a_3 \quad a_4 \,\}^{\mathrm{T}}. \tag{3}$$

The nodal displacements of the element are given by

$$\Delta = \begin{Bmatrix} v_L \\ \theta_L \\ v_R \\ \theta_R \end{Bmatrix} \tag{4}$$

and evaluating the solution at the left and right nodes,

$$\Delta = Pa, \tag{5}$$

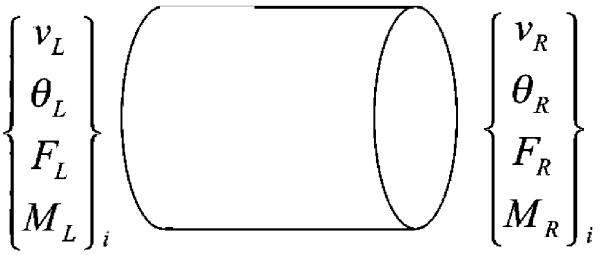

Fig. 3. Shaft geometry.

where P is given by

$$[P] = \begin{bmatrix} 1 & 1 & 1 & 1 \\ -\mathrm{i}k & \mathrm{i}k & -k & k \\ \mathrm{e}^{-\mathrm{i}kL} & \mathrm{e}^{\mathrm{i}kL} & \mathrm{e}^{-kL} & \mathrm{e}^{kL} \\ -\mathrm{i}k\mathrm{e}^{-\mathrm{i}kL} & \mathrm{i}k\mathrm{e}^{\mathrm{i}kL} & -k\mathrm{e}^{-kL} & k\mathrm{e}^{kL} \end{bmatrix}. \tag{6}$$

The nodal forces and moments must satisfy the following at the right and left ends of the beam segment (see Fig. 3):

$$F_L = EIv_{xxxx}|_{x=0}, \tag{7}$$

$$M_L = -EIv_{xxx}|_{x=0}, \tag{8}$$

$$F_R = -EIv_{xxxx}|_{x=L}, \tag{9}$$

$$M_L = EIv_{xxx}|_{x=L}. \tag{10}$$

The nodal forces and moments are

$$F = \begin{Bmatrix} F_L \\ M_L \\ F_R \\ M_R \end{Bmatrix} = \phi a = \phi P^{-1} \Delta, \tag{11}$$

where ϕ is given by

$$\phi = EI \begin{bmatrix} \mathrm{i}k^3 & -\mathrm{i}k^3 & -k^3 & k^3 \\ k^2 & k^2 & -k^2 & -k^2 \\ -\mathrm{i}k^3\mathrm{e}^{-\mathrm{i}kL} & \mathrm{i}k^3\mathrm{e}^{\mathrm{i}kL} & k^3\mathrm{e}^{-kL} & -k^3\mathrm{e}^{kL} \\ -k^2\mathrm{e}^{-\mathrm{i}kL} & -k^2\mathrm{e}^{\mathrm{i}kL} & k^2\mathrm{e}^{-kL} & k^2\mathrm{e}^{kL} \end{bmatrix}. \tag{12}$$

Thus, the stiffness matrix is then given by

$$[K] = \phi P^{-1}. \tag{13}$$

The forces at the ends of the element are related to the displacements by the relation

$$\begin{Bmatrix} F_L \\ M_L \\ F_R \\ M_R \end{Bmatrix} = [K] \begin{Bmatrix} v_L \\ \theta_L \\ v_R \\ \theta_R \end{Bmatrix}. \tag{14}$$

When considering a series of cells, one may derive a relation between consecutive left-end of elements (i to $i+1$). It is given by

$$\begin{Bmatrix} v_L \\ \theta_L \\ F_L \\ M_L \end{Bmatrix}_{i+1} = [T] \begin{Bmatrix} v_L \\ \theta_L \\ F_L \\ M_L \end{Bmatrix}_{i}. \tag{15}$$

Then, the transfer matrix, T, may be constructed using the transformation

$$T = \begin{bmatrix} -K_{LR}^{-1}K_{LL} & K_{LR}^{-1} \\ K_{RR}K_{LR}^{-1}K_{LL} - K_{RL} & -K_{RR}K_{LR}^{-1} \end{bmatrix}, \tag{16}$$

where

$$K = \begin{bmatrix} K_{LL} & K_{RL} \\ K_{LR} & K_{RR} \end{bmatrix}. \tag{17}$$

Thus, the eigenproblem is formulated as

$$[T] \begin{Bmatrix} v_L \\ \theta_L \\ F_L \\ M_L \end{Bmatrix}_{i} = \lambda \begin{Bmatrix} v_L \\ \theta_L \\ F_L \\ M_L \end{Bmatrix}_{i}. \tag{18}$$

Note that the eigenvalues of T occur in pairs λ_i and $1/\lambda_i$, which correspond to the attenuation factor $e^{-\mu}$. Combining the eigenvalue pairs results in a relation by which one may determine μ. By definition of the hyperbolic cosine,

$$e^{-\mu} + e^{\mu} = 2\cosh(\mu) \tag{19}$$

or

$$\mu = a\cosh\left(\frac{e^{\mu} + e^{-\mu}}{2}\right) = a\cosh\left(\frac{\lambda_i + 1/\lambda_i}{2}\right). \tag{20}$$

For the cell geometry shown in Fig. 2 analysis was performed in order to determine the attenuation characteristics. First the geometry was decided. L_A and L_B were chosen to be 10″ each. The diameter of element A was still 1″, but that of element B was made 3″. First, the propagation parameter was determined for the beam cell. Note in Fig. 4 that there are two propagation parameters associated with the beam cell. One corresponds to the near-field waves (both rightward and leftward travelling) and it has a real component for all frequencies. The other is associated with the propagating waves (leftward and rightward travelling). In Figs. 5–7 the magnitudes of the response at the left and right end of a beam (free–free end conditions with a harmonic excitation force at the right end) composed of 1-, 3-, and 5-cell structures are compared. It may be seen that periodic beams composed of greater numbers of cells exhibit the attenuation regions more clearly. Also, when inverting the elements of the cell structure (i.e., B–A rather than A–B), the B–A cell structure does not alter the left-end response, but it does have an appreciable effect on the collocated response at the right end (see Figs. 8–10). Note that the propagation parameter is unaffected by the choice of cell structure (B–A or A–B) for this two element example.

Next, the effects of geometric variations in terms of the cell length ratio (λ_L) were determined for 10″, 20″, and 30″ total cell lengths. The results, plotted against the non-dimensional frequency ($\omega = \bar{\omega}\sqrt{(\rho I_p/GJ)}\bar{L}^2$), are shown in Fig. 11. Increasing the cell length shifts the attenuation regions to lower frequency ranges. Also, the density of attenuation regions increases with increasing cell length.

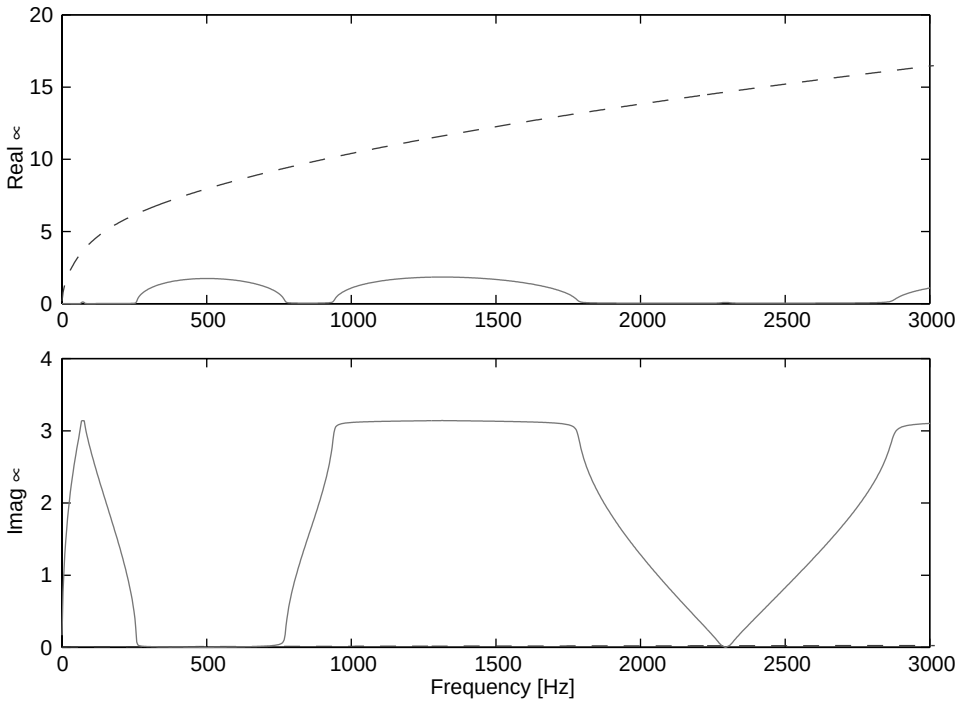

Fig. 4. Propagation parameter for a periodic beam cell: - - -, new field; —, propagating.

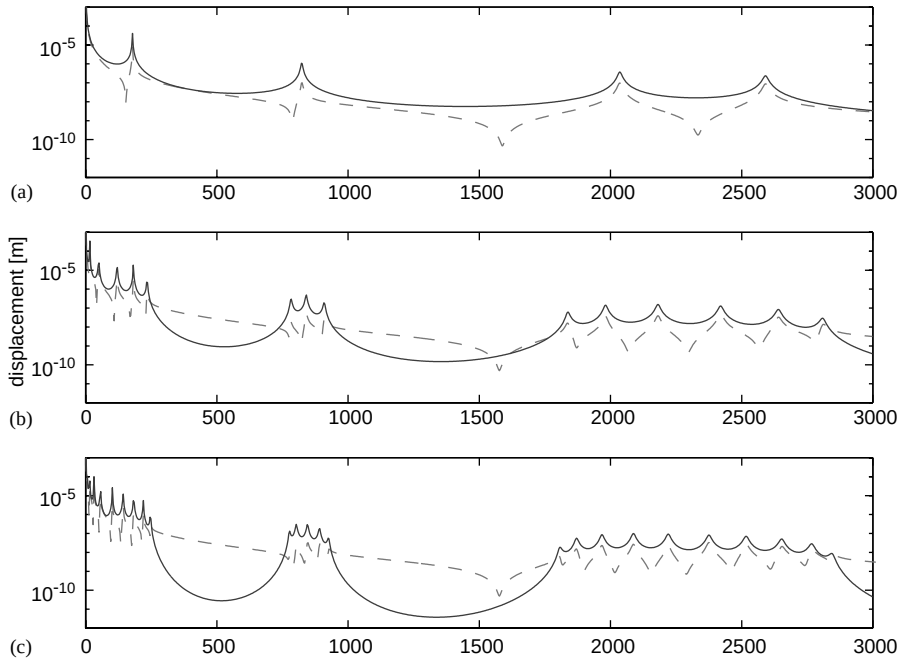

Fig. 5. Magnitude of the left (solid) and right (dashed) ends for (a) 1-, (b) 3-, and (c) 5-cell structures.

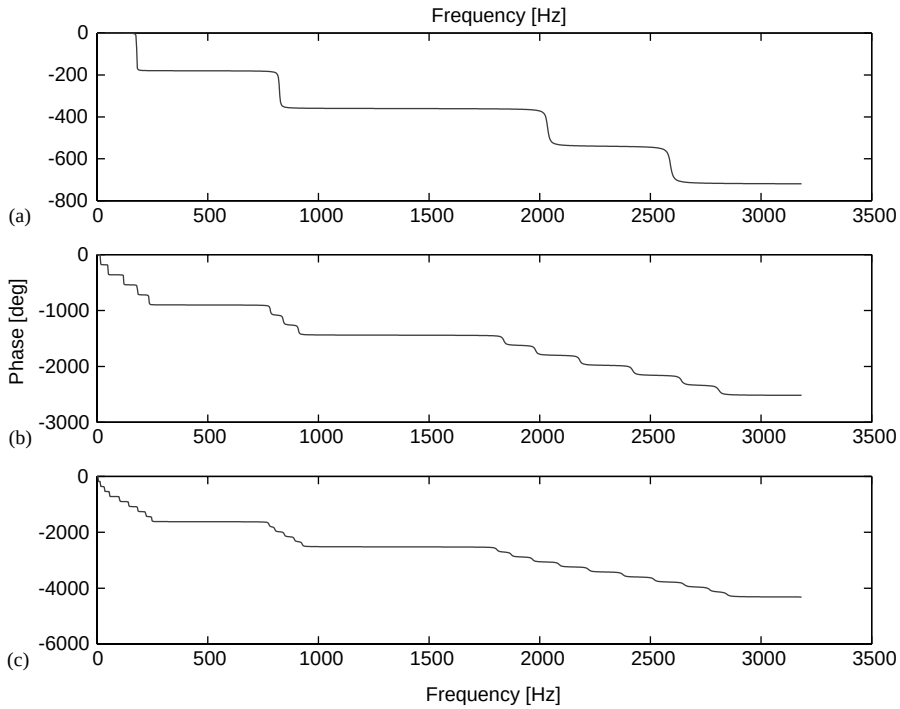

Fig. 6. Phase of the left end displacement for (a) 1-, (b) 3-, and (c) 5-cell structures.

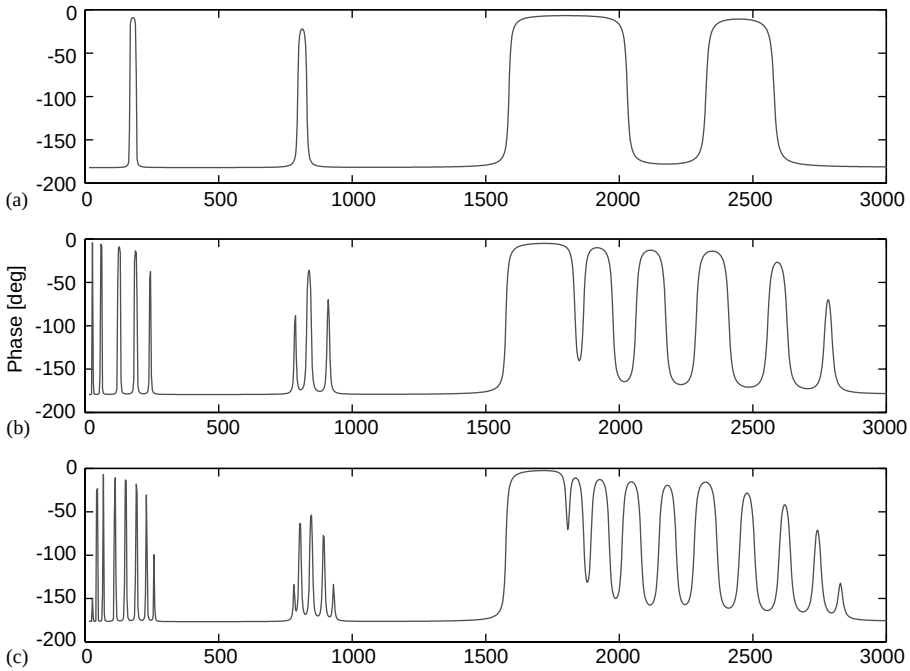

Fig. 7. Phase of right end displacement for (a) 1-, (b) 3-, and (c) 5-cell structures.

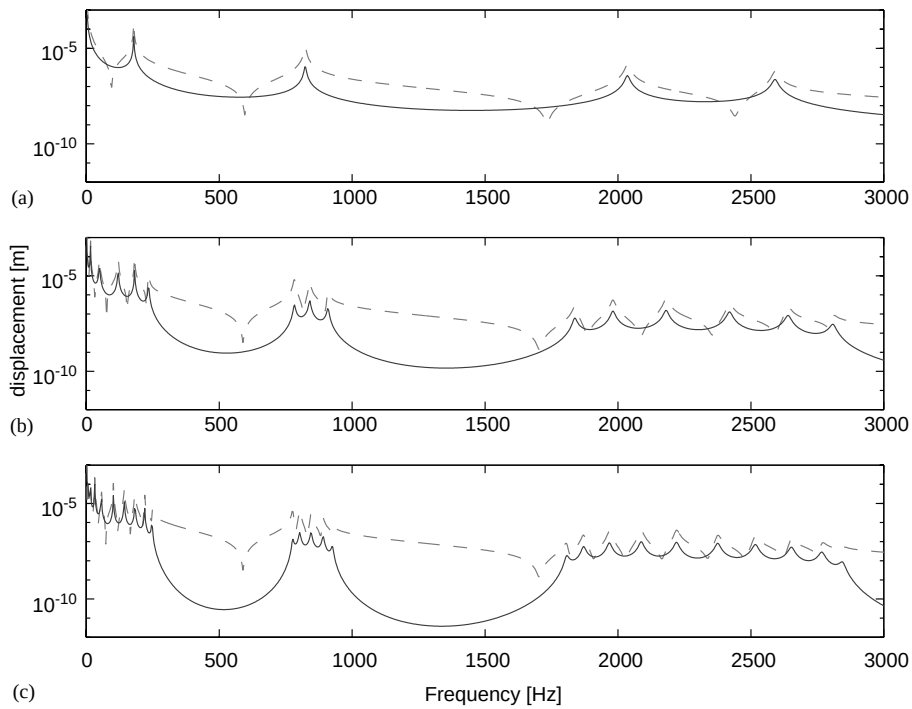

Fig. 8. Magnitude of the left (solid) and right (dashed) ends for (a) 1-, (b) 3-, and (c) 5-cell structures (A and B elements switched).

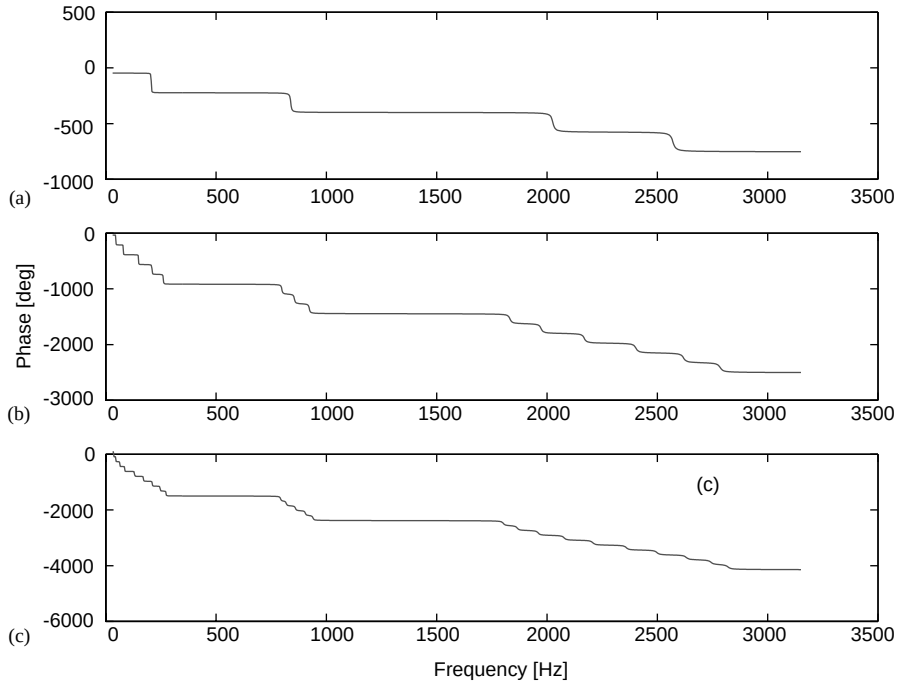

Fig. 9. Phase of left end displacement for (a) 1-, (b) 3-, and (c) 5-cell structures (A and B elements switched).

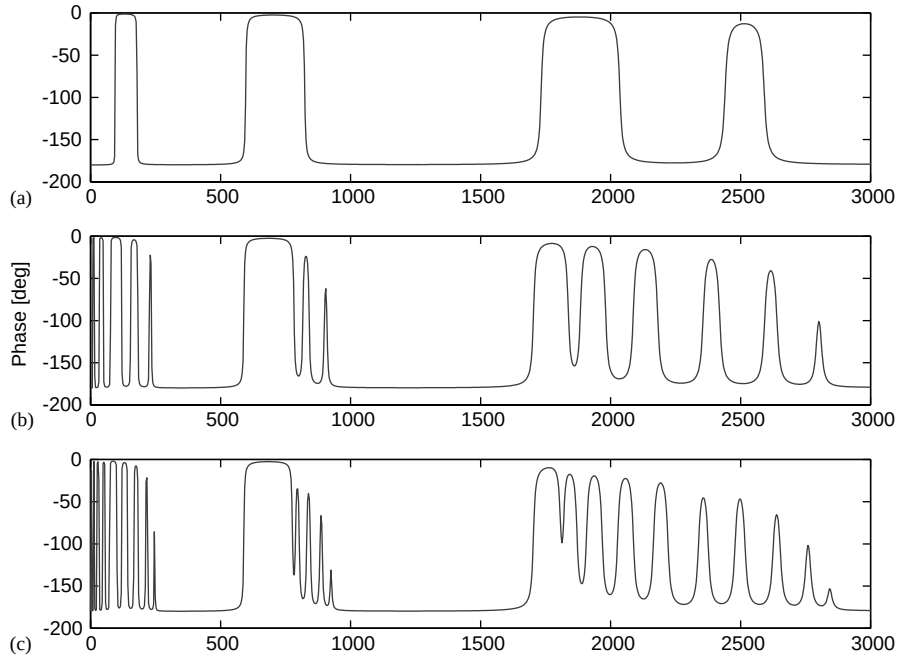

Fig. 10. Phase of right end displacement for (a) 1-, (b) 3-, and (c) 5-cell structures (A and B elements switched).

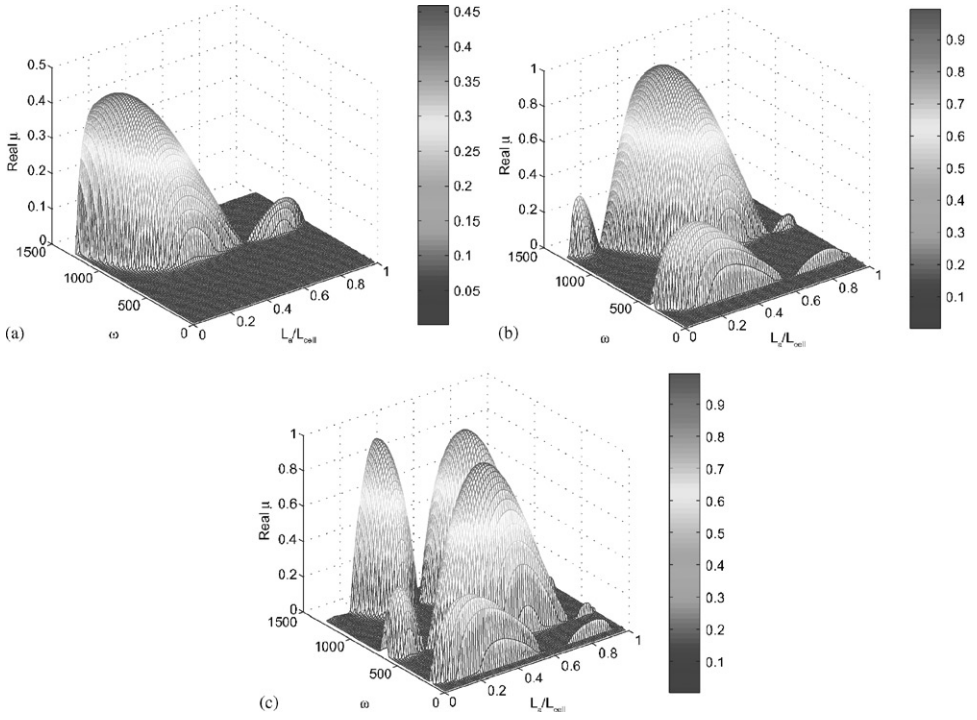

Fig. 11. Real(μ) for various beam cells: (a) $L_{\text{cell}} = 10$ in, (b) 20 in, (c) 30 in.

4. Effect of addition of the gear inertia

Up to this point, the analysis of the periodic shaft has focused on the vibration response of the shaft as a beam. In this initial stage of the research, the rotational effects were not treated in the model. These effects will be added to the analysis in future work. The high stiffness of the shaft and the low rotational velocity of the experiment encouraged the making of the assumption that the rotational effects would be negligible. The main focus of the testing performed for this paper was the verification of the implementation.

In this section, the effects of integrating the gear inertia and boundary conditions are described. To account for the gear inertia, additional elements were added to the transfer function chain of the periodic shaft. Waves are assumed to propagate through the gear elements as if they were part of the same material as the shaft. The element material properties and geometry were made to reflect those of the steel gears available in the lab. The actual configuration for the transverse vibration testing is shown in Fig. 12. The model must also consider the added inertia of the bearings at either end of the shaft in order to accurately predict the propagation parameter. The analysis considers the bearings to be effectively pinned boundary conditions (see Fig. 13).

The shaft was tested in two orientations (see Fig. 14). The propagation parameter for the periodic shaft in both configurations are shown in Figs. 15 and 16. Note that there are attenuation regions at lower frequencies for the periodic shaft including the bearing and gear inertias than for the shaft without their inclusion (see Fig. 17). The propagation parameter of a uniform shaft with the mass of the gear added is shown in Fig. 18. Note that although the shaft alone has no

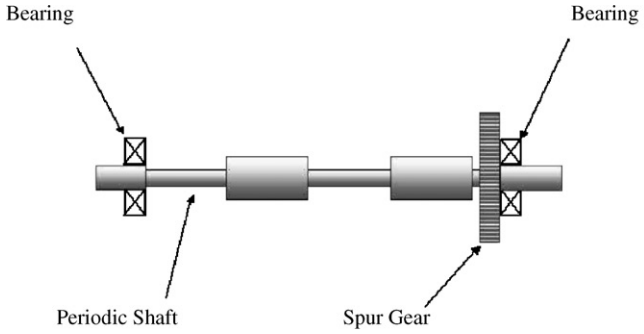

Fig. 12. Driven shaft with gear and bearing shown.

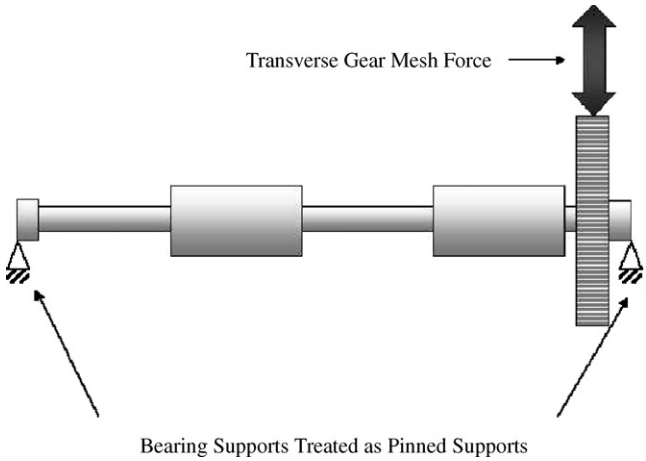

Fig. 13. Driven shaft analytical model.

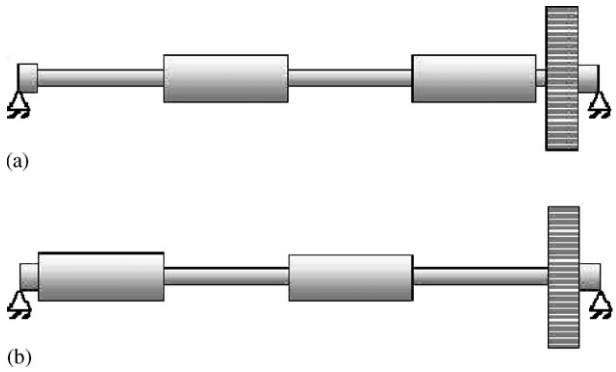

Fig. 14. (a) Primary and (b) inverted configurations.

attenuation regions, that with the addition of the gear inertia introduces attenuation regions, albeit very small. Thus, the addition of inertia is beneficial in terms of the propagation parameter, causing additional attenuation regions to appear at lower frequencies.

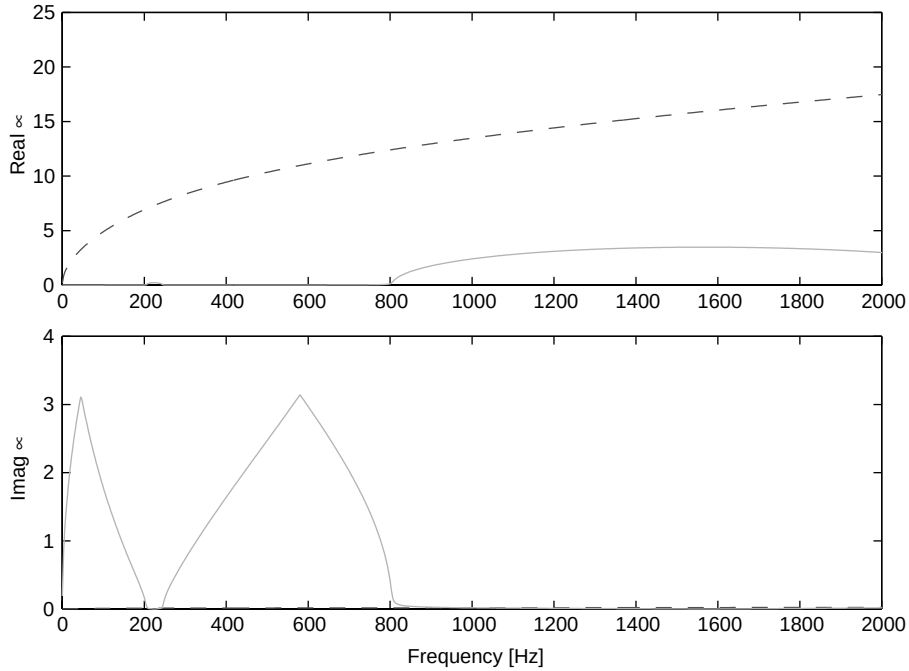

Fig. 15. Propagation parameter for periodic shaft without bearing and gear inertia included: - - -, new field; —, propagating.

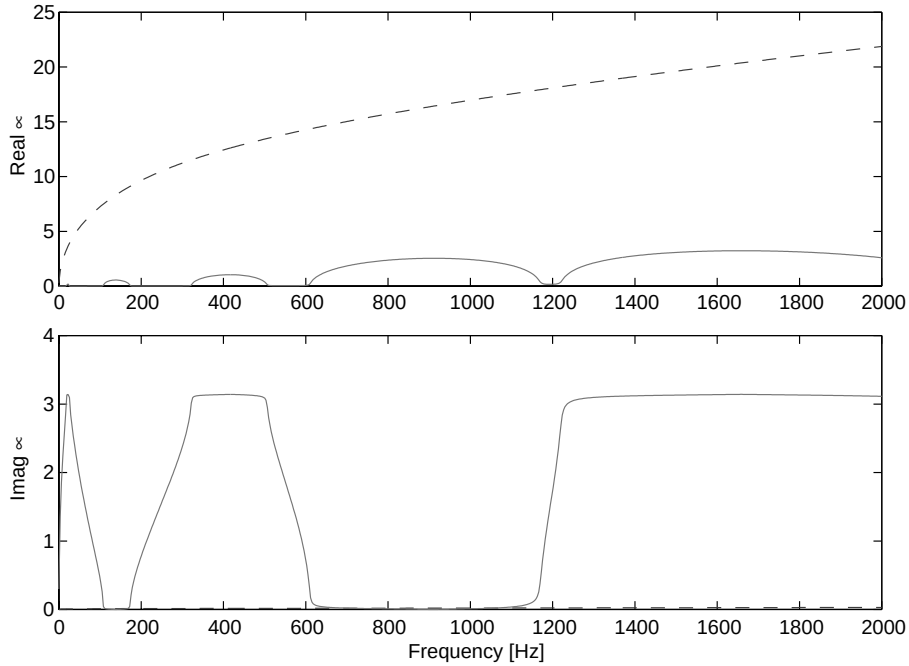

Fig. 16. Propagation parameter for periodic shaft: - - -, new field; —, propagating.

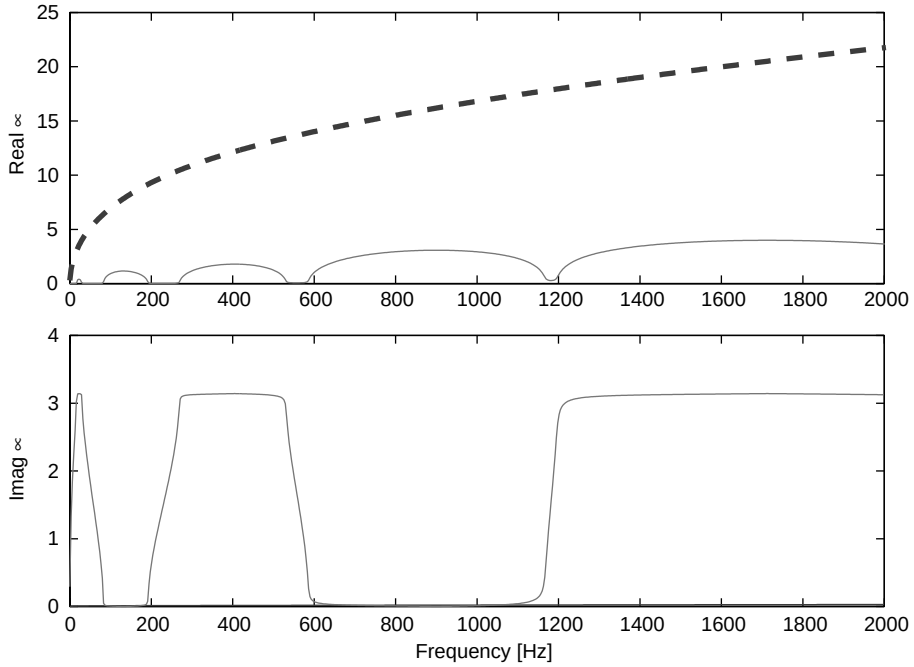

Fig. 17. Propagation parameter for inverted periodic shaft: - - -, new field; —, propagating.

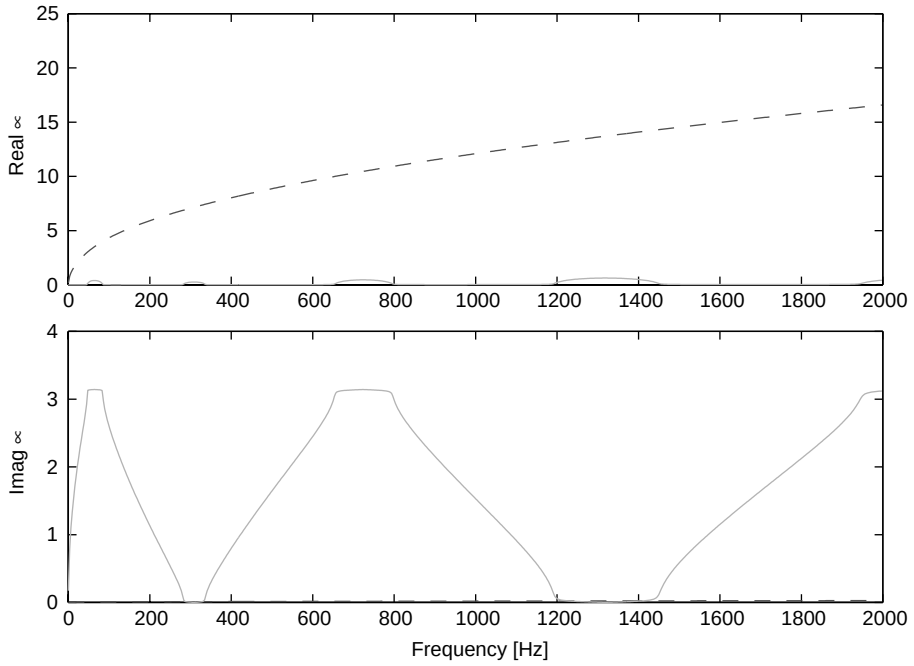

Fig. 18. Propagation parameter for uniform shaft with gear inertia included: - - -, new field; —, propagating.

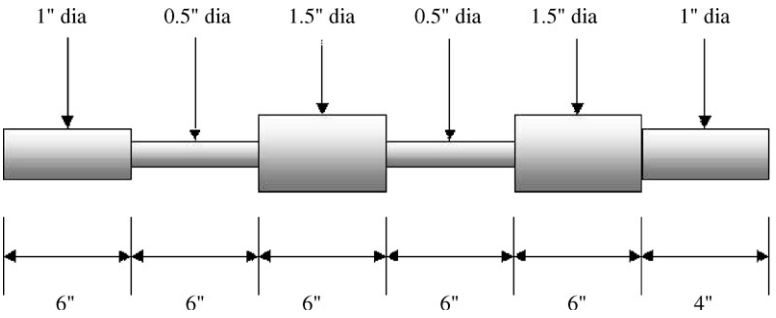

Fig. 19. Periodic test shaft geometry.

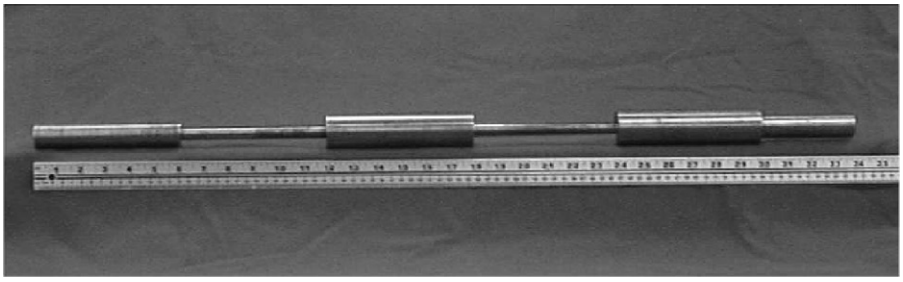

Fig. 20. Periodic shaft.

5. Transmission test rig set-up

A periodic shaft was fabricated to integrate with a spur gear system (see Figs. 19 and 20). The University of Maryland Transmission Test Rig (see Fig. 21) was used to evaluate the performance of the periodic shaft. The spur gear pair had a 1:1 gear ratio and 50 teeth per gear. There was a 5 in pitch diameter and a contact ratio of 1.75. Any reduction of transmitted vibrations generated by gear tooth contact would be measured at the bearing supports. The test instrumentation for the transmission rig tests are shown in Figs. 21–23.

6. Periodic shaft design

To evaluate the attenuation properties of a periodic shaft, a periodic shaft was manufactured and mounted between two bearings. At one end, a spur gear was attached and allowed to engage with another spur gear. Two accelerometers were attached to each bearing support. A comparison of the acceleration response vector at these two bearing supports will demonstrate the attenuation characteristics of the shaft. The drive motor of the test rig was run at several operating speeds, thus generating a variety of mesh excitation frequencies. The periodic shaft was tested in both orientations as well as a uniform shaft for comparison purposes (see Table 1 for a comparison of the shafts). Table 2 shows the operating speeds and torque loads that were used to evaluate the performance of the periodic shaft.

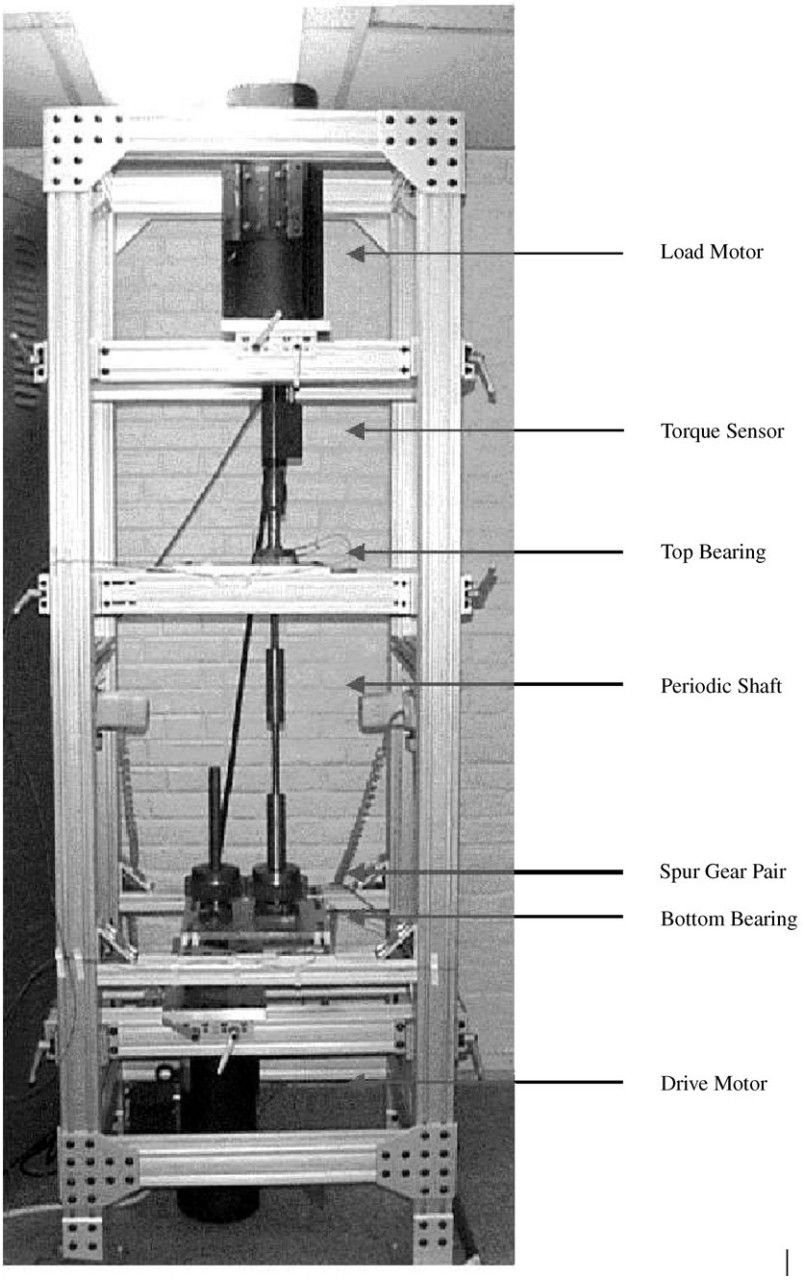

Fig. 21. Transmission test rig.

The attenuation properties in bending of the shaft are indicated in Fig. 24 (the primary configuration) and Fig. 25 (the inverted configuration). These two configurations are defined in Fig. 14. Notice that strong attenuation is achieved in the frequency range from 600 to 1200 Hz

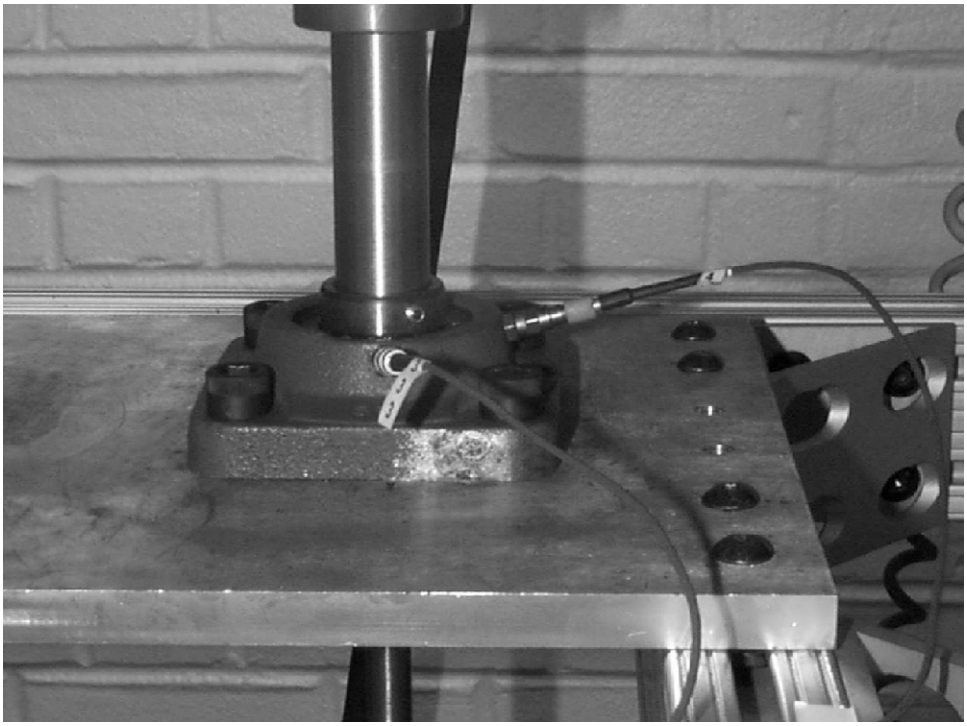

Fig. 22. Accelerometer placement at top bearing.

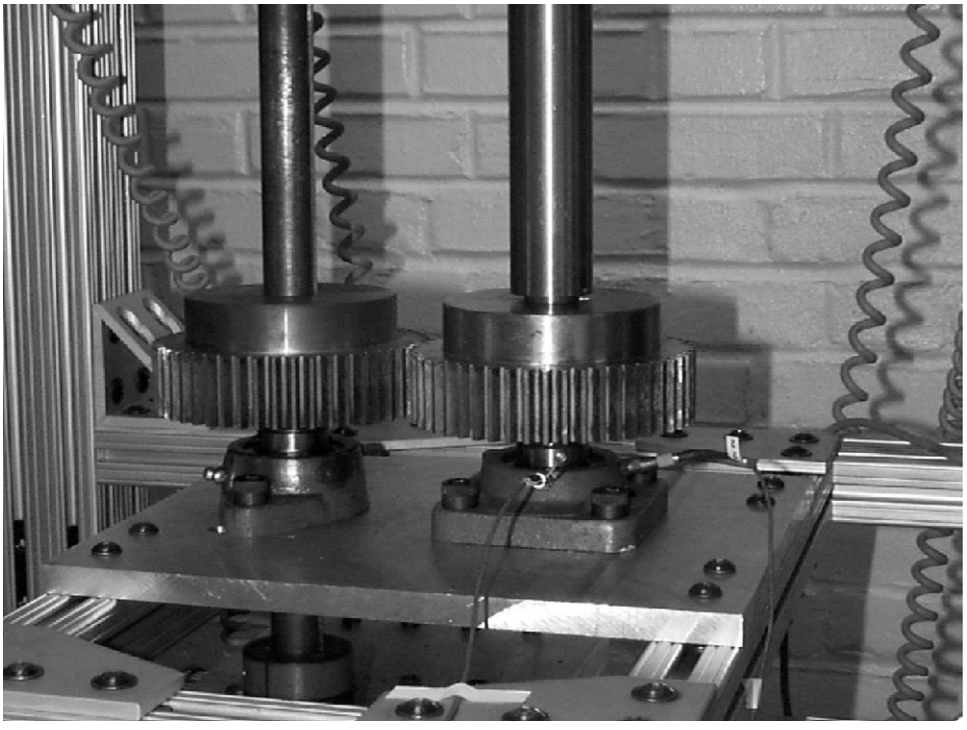

Fig. 23. Accelerometer placement at bottom bearing.

Table 1
Comparison of periodic and uniform shafts

	Periodic	Periodic (Inverted)	Uniform
Weight	3.03 kg	3.03 kg	2.42 kg
Stiffness	268.2 N m^2 (0.5″ dia)	268.2 N m^2 (0.5″ dia)	4290.7 N m^2
(EI)	21 721.5 N m^2 (1.5″ dia)	21 721.5 N m^2 (1.5″ dia)	
Length	27″	27″	27″
Shaft resonances	36.5 Hz	35.5 Hz	111.3 Hz
(with gear	176.5 Hz	136.9 Hz	444.9 Hz
and bearing	500.0 Hz	350.5 Hz	1002.0 Hz
inertias)	1750.2 Hz	633.01 Hz	1781.1 Hz

Table 2
Experimental operating speeds and measured torque loads

Operating speed (r.p.m.)	Torque load (periodic shaft) (in lb)	Torque load (periodic shaft inverted) (in lb)	Torque load (uniform shaft) (in lb)
100	20	26	34
150	37	44	50
200	54	70	68
250	72	84	88
300	90	103	101
350	106	118	123
400	122	133	143
450	139	153	161

and 1250 to 2000 Hz for both configurations, though the inverted configuration should exhibit stronger attenuation and slightly larger attenuation zones.

7. Experimental results

Experimental results for testing the periodic shaft were obtained at a variety of rotation rates. Representative results are presented for the 450 r.p.m. case. The acceleration at each bearing for a given shaft are compared as well as comparisons of the uniform and periodic shafts at a given bearing in Figs. 26–33. The level of attenuation varies with r.p.m. as well as configuration of the periodic shaft (primary or inverted). For the primary configuration, there is attenuation achieved at the top bearing but only at the expense of increased vibration at the bottom bearing. The inverted shaft shows attenuation at either bearing and is therefore shown to be the superior configuration. The same general attenuation characteristics occur at all operating speeds. However, at low operating speeds, the magnitude of forces is small, and, for higher frequencies, the magnitude of the vibration at either bearing is on the order of the noise of the system and the attenuation characteristics of the shaft are not readily apparent. For the shaft in the primary configuration, the analysis shows attenuation regions between 400 and 500 Hz, 600 and 1150 Hz,

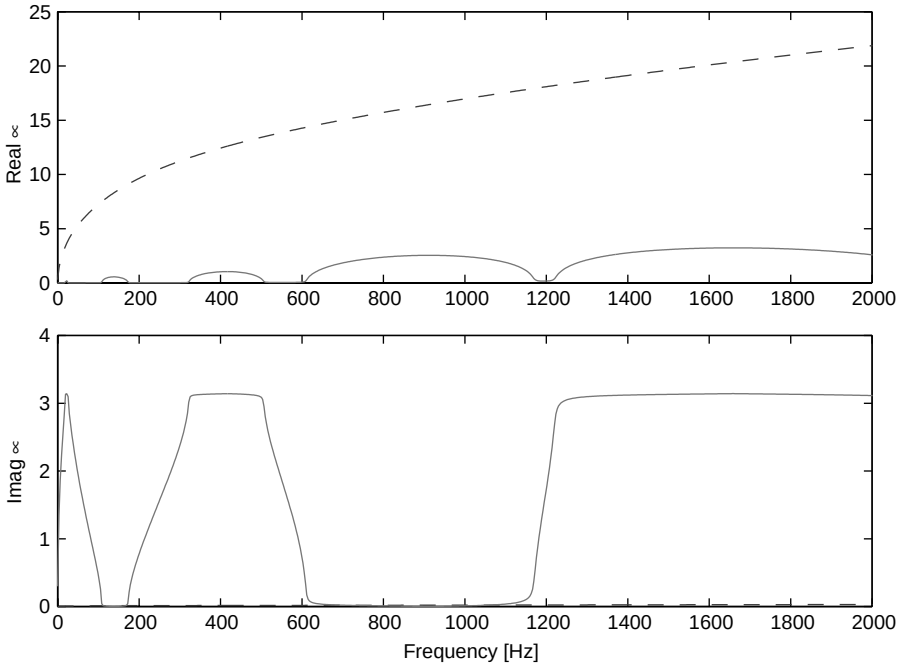

Fig. 24. Periodic shaft propagation parameter: - - -, new field; —, propagating.

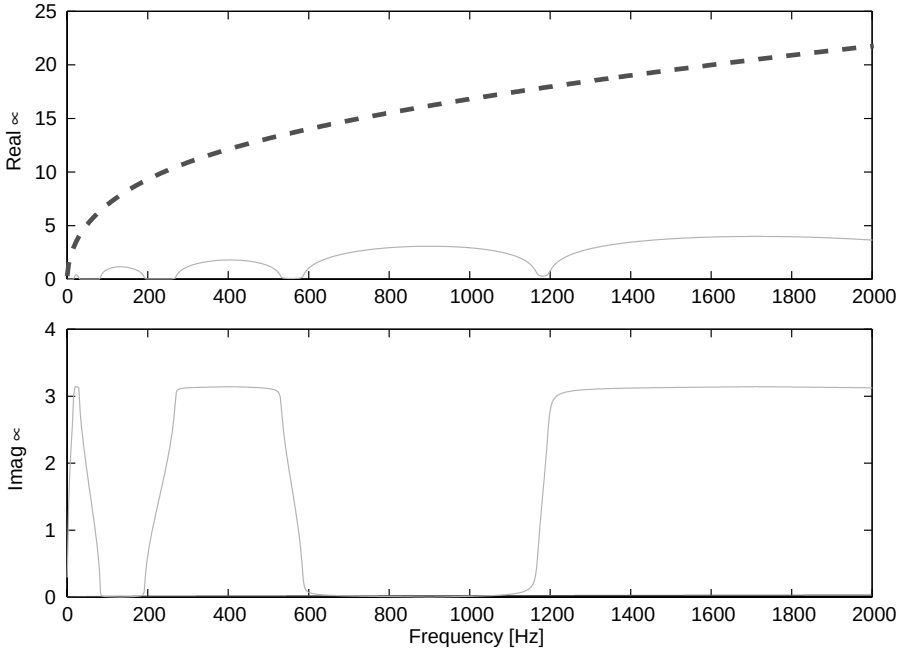

Fig. 25. Periodic shaft propagation parameter (inverted shaft): - - -, new field; —, propagating.

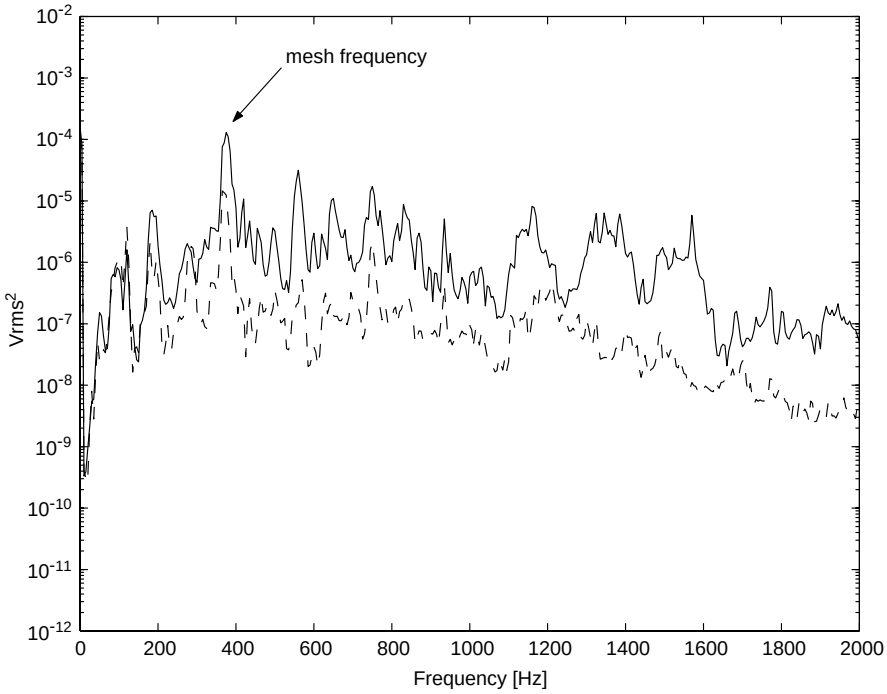

Fig. 26. Experimental results for the periodic shaft at 450 r.p.m.: —, bottom bearing; - - -, top bearing.

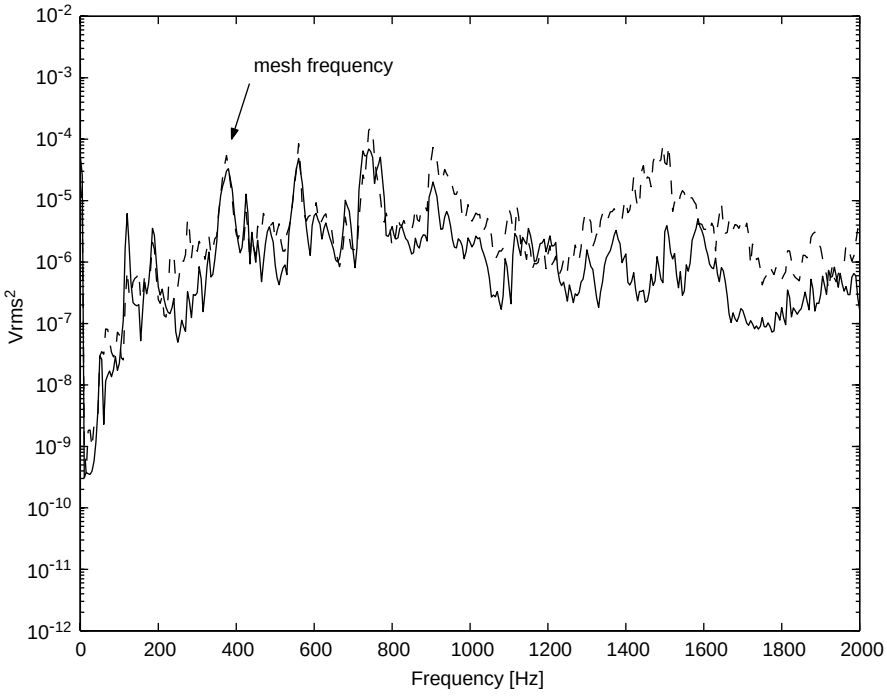

Fig. 27. Experimental results for the uniform shaft at 450 r.p.m.: —, bottom bearing; - - -, top bearing.

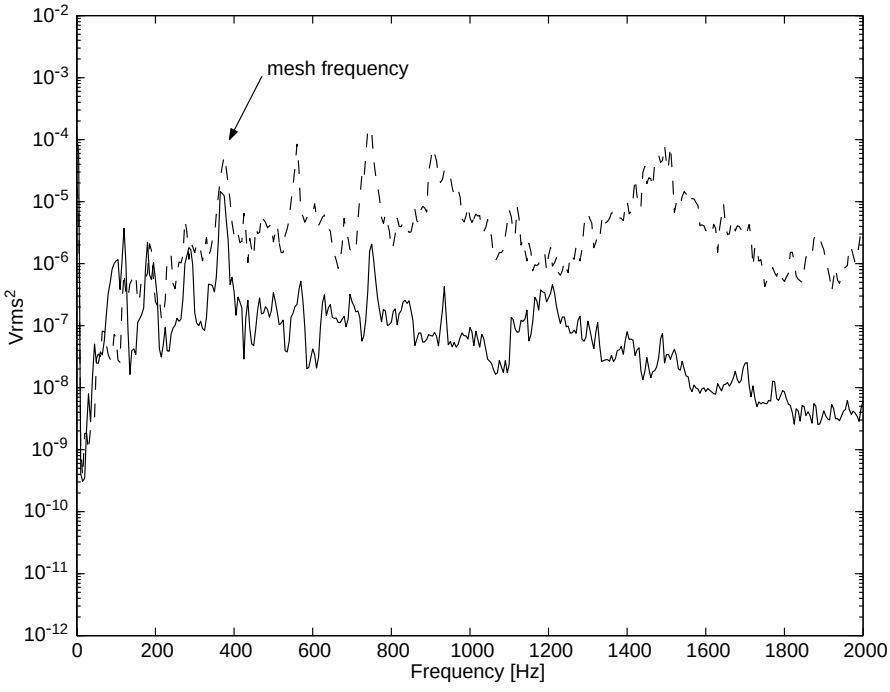

Fig. 28. Experimental results for the top bearing at 450 r.p.m.: —, periodic; - - -, uniform.

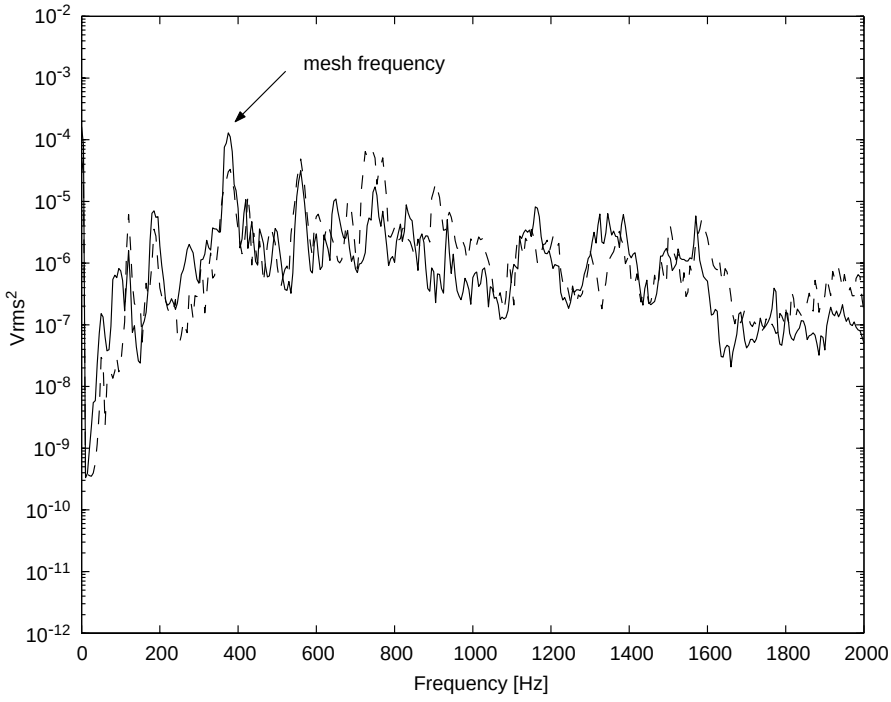

Fig. 29. Experimental results for the bottom bearing at 450 r.p.m.: —, periodic; - - -, uniform.

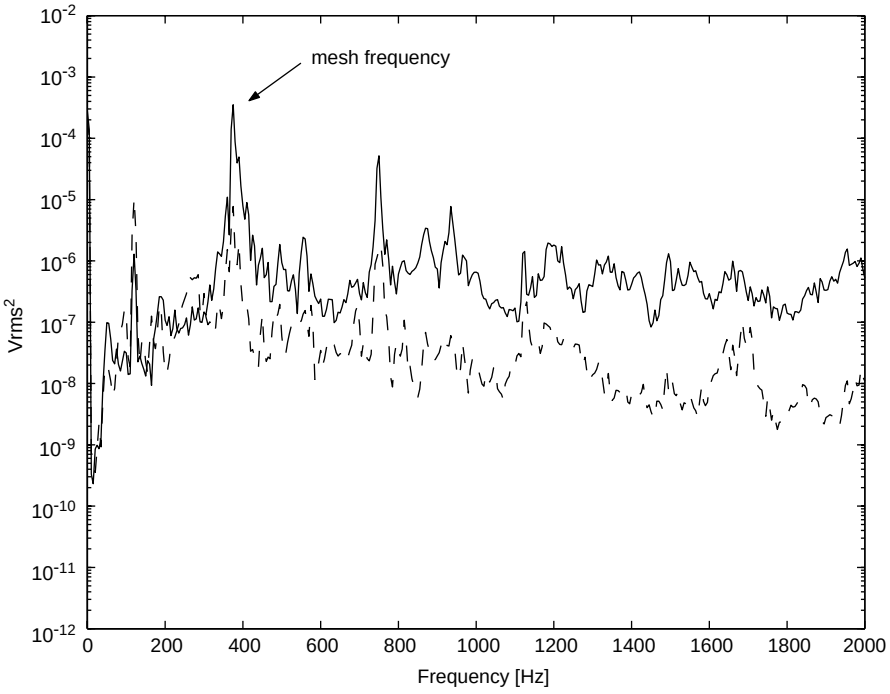

Fig. 30. Experimental results for the periodic shaft (inverted configuration) at 450 r.p.m.: —, periodic; - - -, uniform.

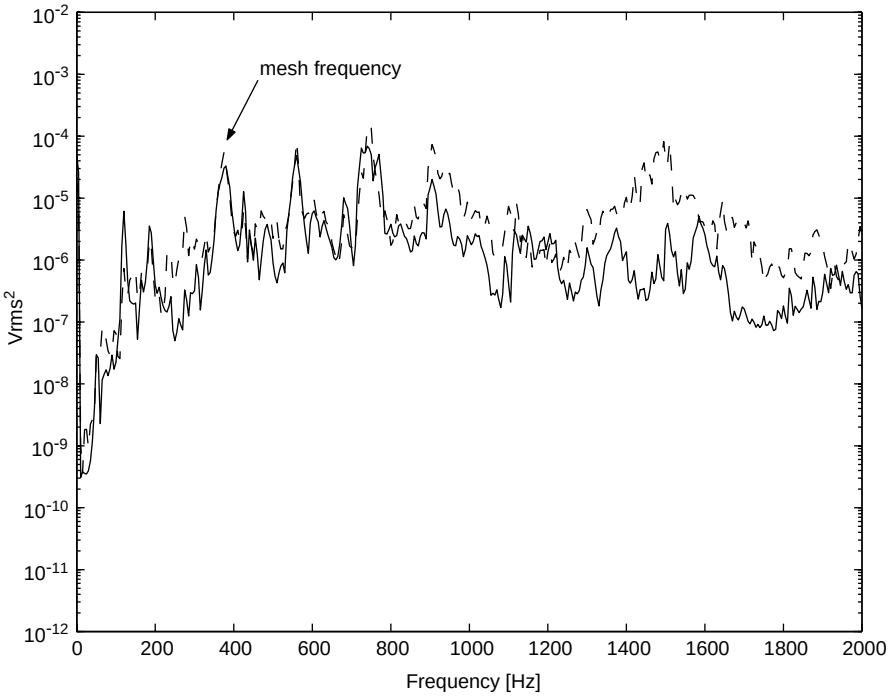

Fig. 31. Experimental results for the uniform shaft at 450 r.p.m.: —, bottom bearing; - - -, top bearing.

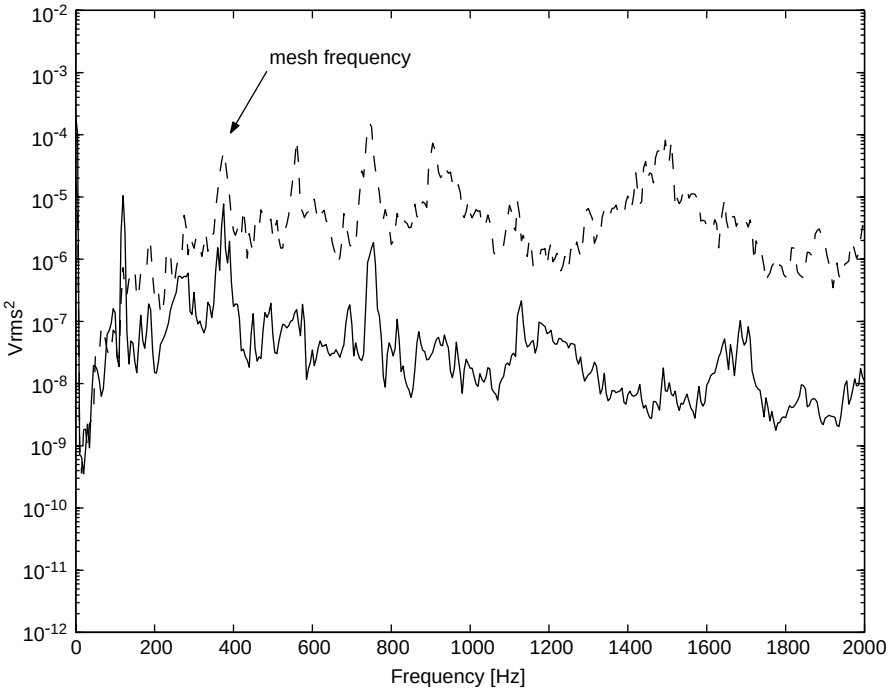

Fig. 32. Experimental results for the top bearing at 450 r.p.m. (with periodic shaft in inverted configuration): —, periodic; - - -, uniform.

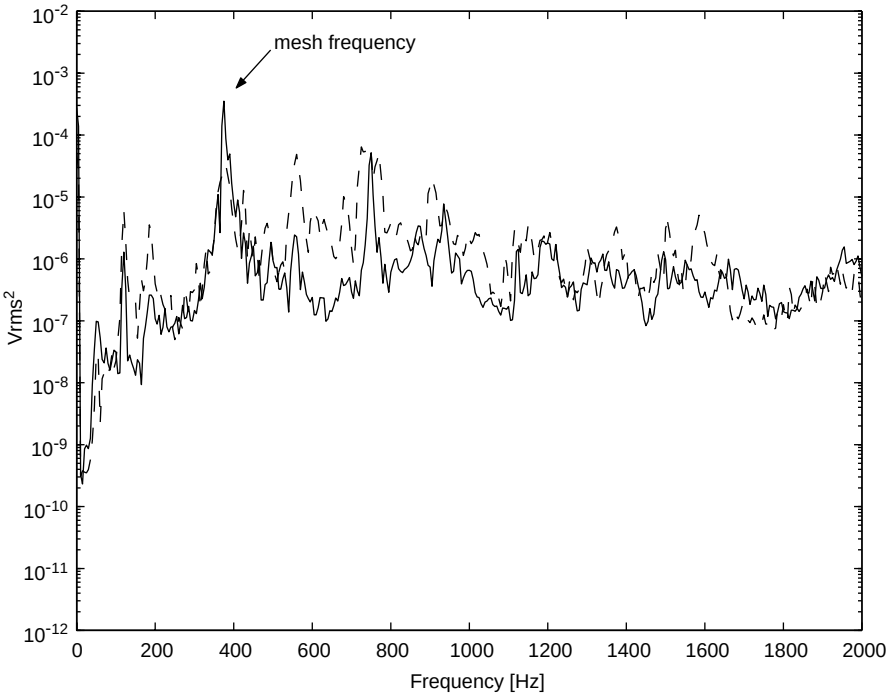

Fig. 33. Experimental results for the bottom bearing at 450 r.p.m. (with periodic shaft in inverted configuration): —, periodic; - - -, uniform.

and 1250–2000 Hz. The region between 1150 and 1250 Hz, where a pass band exists is plainly visible in the test data. For the inverted-shaft configuration, the pass bands between the stop bands are also visible. There are attenuation regions for the uniform shaft which the analysis failed to predict. In the frequency bands of 500–600 Hz and 1500–1700 Hz, there are clear indications of attenuation. However, the analysis predicts only small attenuation regions and at different frequencies. Future work should address this issue to determine the cause of these attenuation regions.

Tables 3 and 4 demonstrate the overall attenuation characteristic of the shafts considered. Table 3 compares the power of the signals across the frequency band considered at the bearings. This was calculated as the area under the frequency spectra. The ratio of the acceleration at the top bearings to that at the bottom bearing gives some indication of the level of attenuation for the shaft considered. Overall, the periodic shaft in the primary configuration appears to provide the greatest end-to-end attenuation. But recall that the vibration level at the bottom bearing for this configuration was higher than the inverted configuration and the uniform shaft. Table 4 compares the periodic shaft in both configurations to the uniform shaft. With the uniform shaft as a reference, it may be inferred that the inverted-shaft configuration results in the lowest overall vibration level at both bearings.

Table 3
Summary table of reduction achieved

Operating speed (r.p.m.)	Periodic shaft	Periodic shaft (inverted)	Uniform shaft
100	71.03%↓	75.40%↓	17.92%↓
150	77.72%↓	54.94%↓	59.31%↓
200	84.13%↓	80.94%↓	25.83%↓
250	83.59%↓	93.73%↓	60.01%↓
300	89.40%↓	65.29%↓	75.84%↓
350	83.59%↓	64.27%↓	40.83%↓
400	88.02%↓	90.20%↓	22.64%↑
450	90.53%↓	94.41%↓	121.79%↑

Table 4
Summary table of reduction achieved with respect to the uniform shaft

Operating speed (r.p.m.)	Periodic shaft Bottom bearing	Periodic shaft Top bearing	Periodic shaft (inverted) Bottom bearing	Periodic shaft (inverted) Top bearing
100	3.54%↓	65.96%↓	81.06%↓	94.32%↓
150	45.26%↓	70.03%↓	83.85%↓	82.12%↓
200	17.70%↓	82.39%↓	79.49%↓	94.73%↓
250	26.66%↓	69.91%↓	73.77%↓	95.89%↓
300	70.88%↓	87.22%↓	89.61%↓	85.07%↓
350	20.97%↓	78.09%↓	71.69%↓	82.91%↓
400	10.90%↓	91.29%↓	69.01%↓	97.52%↓
450	18.52%↓	96.52%↓	28.18%↓	98.19%↓

8. Conclusions

The goal of this research has been to demonstrate the use of periodic structures in drivetrains in order to reduce the mesh frequency vibrations and their higher harmonics from being transmitted through structural components. First a dynamic model was developed and then used to simulate an operating system and predict the excitation forces generated at the meshing point. Next, a spectral finite element analysis method was used to determine the frequency spectra and propagation parameters for beams with geometric periodicity in the longitudinal direction. Then a periodic shaft was fabricated and tested in the University of Maryland Transmission Test Rig. The analysis proved to closely predict the attenuation properties of the test shaft. The test data shows distinct attenuation regions for the periodic shaft which do not appear for a uniform shaft. Test results showed that it is possible to not only reduce the transmitted vibrations along the shaft, but also those at the point of application of the excitation force. The present work has only considered the use of an isotropic structure. Future work may focus on the use of shafts with material property variations as well as geometric. In a transmission system for a helicopter, the supporting struts might also be designed using the analytical tools presented in this paper to filter out frequency bands critical to reducing vibration transmitted from the gearbox.

Appendix A. Nomenclature

E	Young's modulus
I	moment of inertia
v	transverse beam deflection
K	dynamic stiffness matrix
T	cell transfer matrix
$L_{a,b}$	element length
λ_L	cell length ratio (L_a/L_b)
μ	propagation parameter
$\bar{\omega}$	frequency (rads/s)
ω	non-dimensionalized frequency

References

[1] J.D. Smith, Gear Noise and Vibration, Marcel Dekker, New York, 1999.
[2] F.B. Oswald, J.J. Zakrajsed, D.P. Townsend, W. Atherton, H.H. Lin, Effect of operating conditions on gearbox noise, in: International Power Transmission and Gearing Conference, Vol. 2, ASME, New York, 1992, pp. 669–674.
[3] M.A. Arikan, Effect of addendum modification of spur gear dynamic loads, in: International Power Transmission and Gearing Conference, Vol. 88, ASME, New York, 1996, pp. 1–8.
[4] Y. Cai, T. Hayashi, The optimum modification of tooth profile for a pair of spur gears to make its rotational vibration equal to zero, in: International Power Transmission and Gearing Conference, Vol. 2, ASME, New York, 1992, pp. 453–460.

[5] D.R. Houser, The root of gear noise-transmission error, Power Transmission Design 5 (1986) 27–30.
[6] W.S. Rouverol, New modifications eradicate gear noise and dynamic increment at all loads, in: International Power Transmission and Gearing Conference, Vol. 88, ASME, New York, 1996, pp. 17–21.
[7] K. Inoue, D.P. Townsend, J.J. Coy, Optimum design of a gearbox for low vibration, in: International Power Transmission and Gearing Conference, Vol. 2, ASME, New York, 1992, pp. 497–504.
[8] H. Okamura, Y. Suzuki, N. Nakano, Experiments and analysis of sound-damping rings for gears, in: Power Transmission and Gearing Conference, Vol. 88, ASME, New York, 1996, pp. 345–354.
[9] E. Luft, B. Balachandran, Interior noise control using smart materials, Presented at the ARO Workshop on Smart Structures, 1999.
[10] T. Millott, W.W.C. Yoerkie, D. MacMartin, M. Davis, Flight test of active gear-mesh noise control on the S-76 aircraft, in: Proceedings at the American Helicopter Society 54th Annual Forum, Washington, DC, May 1998.
[11] G.T. Montague, A.F. Kascak, A. Palazzolo, D. Manchala, E. Thomas, Feed-forward control of gear mesh vibration using piezoelectric actuators, Technical Report 1.5:106366, NASA, 1994.
[12] I. Pelinescu, B. Balachandran, Analytical study of active control of wave transmission through cylindrical struts, Smart Materials and Structures 10 (2001) 121–136.
[13] W. Gembler, H. Schweitzer, Helicopter interior noise reduction by active gearbox struts, in: Proceedings at the American Helicopter Society 54th Annual Forum, Washington, DC, May 1998.
[14] A.C. Lee, S.-T. Chen, Optimal vibration control for a flexible rotor with gyroscopic effects, JSME International Journal 35 (3) (1992) 446–455.
[15] K. Nonami, T. Yamanaka, M. Tominaga, Vibration and control of a flexible rotor supported by magnetic bearings, JSME International Journal 33 (4) (1990) 475–482.
[16] H. DeSmidt, K. Wang, E. Smith, Active vibration control of rotorcraft driveshaft-airframe dynamics, in: Proceedings at the American Helicopter Society 54th Annual Forum, Washington, DC, May 1998.
[17] J.C. Jauregui, J.A. Becerril, A.L. Guzman, Viscoelastic torsional damper model, in: Power Transmission and Gearing Conference, Vol. 88, ASME, New York, 1996, pp. 777–780.
[18] I.Y. Shen, W. Guo, Y.C. Pao, Torsional vibration control of a shaft through active constrained layer damping treatments, Journal of Vibration and Acoustics 119 (1999) 504–511.
[19] L. Brillouin, Wave Propagation in Periodic Structures, Dover, New York, 1953.
[20] D.J. Mead, A general theory of harmonic wave propagation in linear periodic systems with multiple coupling, Journal of Sound and Vibration 27 (1973) 235–260.
[21] D.J. Mead, Vibration response and wave propagation in periodic structures, Journal of Engineering for Industry 21 (1971) 783–792.
[22] D.J. Mead, Wave propagation and natural modes in periodic systems: I. Mono-coupled systems, Journal of Sound and Vibration 40 (1) (1975) 1–18.
[23] D.J. Mead, Wave propagation and natural modes in periodic systems: II. Multi-coupled systems, with and without damping, Journal of Sound and Vibration 40 (1) (1975) 19–39.
[24] R.M. Orris, M. Petyt, A finite element study of harmonic wave propagation in periodic structures, Journal of Sound and Vibration 33 (2) (1974) 223–237.
[25] B. Ravindra, K. Mallik, Harmonic vibration isolation characteristics of periodic systems, Journal of Sound and Vibration 154 (2) (1992) 249–259.
[26] J.F. Doyle, Wave Propagation in Structures, Springer, New York, 1997.
[27] M. Ruzzene, A. Baz, Attenuation and localization of wave propagation in periodic rods using shape memory inserts, 2000, unpublished.
[28] M. Ruzzene, A. Baz, Control of wave propagation in periodic composite rods using shape memory inserts, Journal of Vibration and Acoustics 122 (2000) 151–159.